Accepted Manuscript

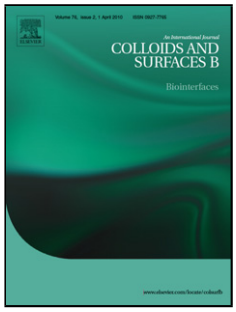

Title: Electrochemical biosensor based on Se-doped MWCNTs-graphene and Y-shaped DNA-aided target-triggered amplification strategy

Authors: Yi-Han Wang, Ying-Xu Chen, Xu Wu, Ke-Jing Huang

PII: S0927-7765(18)30599-X
DOI: https://doi.org/10.1016/j.colsurfb.2018.08.064
Reference: COLSUB 9596

To appear in: *Colloids and Surfaces B: Biointerfaces*

Received date: 2-6-2018
Revised date: 25-8-2018
Accepted date: 29-8-2018

Please cite this article as: Wang Y-Han, Chen Y-Xu, Wu X, Huang K-Jing, Electrochemical biosensor based on Se-doped MWCNTs-graphene and Y-shaped DNA-aided target-triggered amplification strategy, *Colloids and Surfaces B: Biointerfaces* (2018), https://doi.org/10.1016/j.colsurfb.2018.08.064

Electrochemical biosensor based on Se-doped MWCNTs-graphene and Y-shaped DNA-aided target-triggered amplification strategy

Yi-Han Wang [a], Ying-Xu Chen [a], Xu Wu [b], Ke-Jing Huang [a,*]

[a] *College of Chemistry and Chemical Engineering, Xinyang Normal University, Xinyang 464000, China*

[b] *School of Physics and Electronic Engineering, Xinyang Normal University, Xinyang 464000, China*

[*]Corresponding author. Tel.: +86-376-6390611

E-mail address: kejinghuang@163.com (K.J. Huang)

Graphic abstract

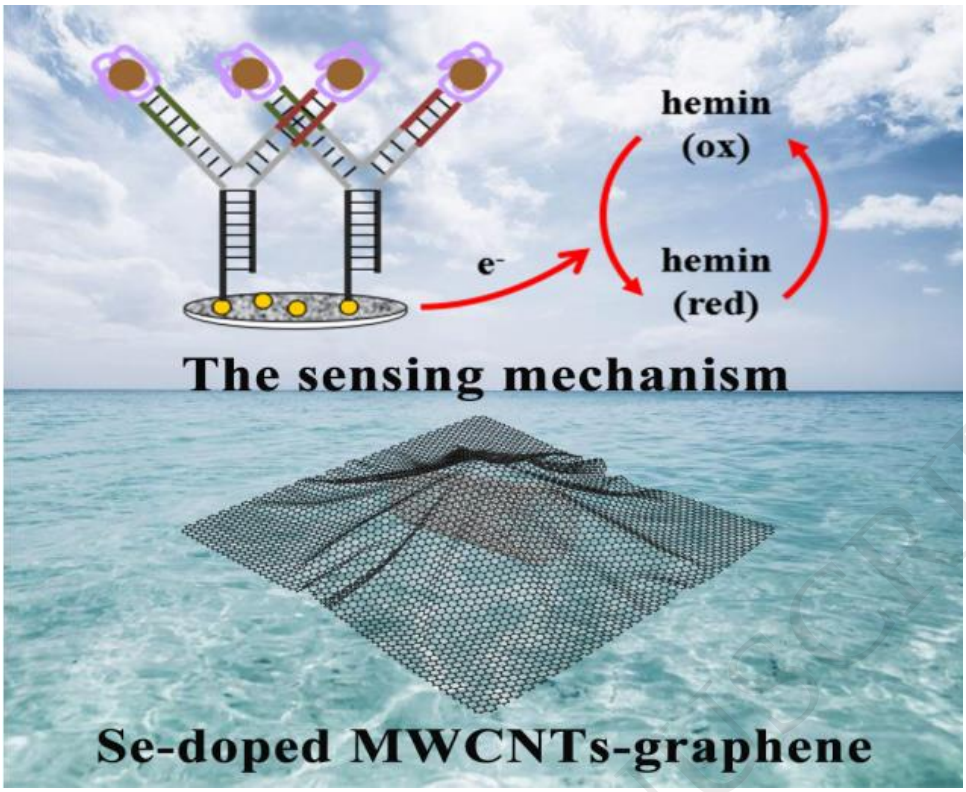

Highlights

- • Se doping MWCNTs-graphene hybrids are prepared and used for supporting substrate.
- • Y-shaped DNA-aided target recycling signal amplification and hemin/G-quadruplex is used for signal amplification.
- • The biosensor used for PDGF-BB detection shows linear range of 0.1 pM-10 nM and detection limit of 27 fM.

ABSTRACT:

A highly sensitive electrochemical biosensor for detection of platelet-derived growth factor-BB (PDGF-BB) is developed by using Se-doped multi-walled carbon nanotubes (MWCNTs)-graphene hybrids as electrode supporting substrate, hemin/G-quadruplex as trace labels and Y-shaped DNA-aided target recycling as signal magnifier. The aptamer-containing hairpin probes were first immobilized on the electrode. When target PDGF-BB was added, the aptamer binded PDGF-BB to trigger catalytic assembly of two other hairpins to form many G-quadruplex Y-junction DNA structures, which released PDGF-BB to again bind the intact aptamer to initiate another assembly cycle. G-quadruplex/hemin complexes were produced when hemin was added to generate substantially amplified current output. The developed assay showed a linear range toward PDGF-BB from 0.1 pM to 10 nM with a detection limit of 27 fM (S/N=3). The method showed excellent specificity and repeatability, and could be expediently applied for sensitive detection of other molecules by simply changing the aptamers.

Keywords: Signal amplification; Hemin/G-quadruplex; Y-shaped DNA; Platelet-derived growth factor-BB

1. Introduction

Platelet derived growth factor-BB (PDGF-BB) relates to some appalling diseases, such as atherosclerosis, fibrosis, and many cell transformation and tumor growth processes [1]. Usually, its content in inchoate stage of one disease is very low [2], so it is necessary to develop sensitive and selective methods for its detection [3]. Different assays have been developed for PDGF-BB detection, such as fluorescent assays [4], chemiluminescence [5], colorimetric [6] and electrochemical methods [7]. For improving the selectivity, antibodies and aptamers have been widely used in these methods. However, the critical in vivo synthesis conditions of antibodies have limited their applications. Aptamers are DNA/RNA oligonucleotides selected from combinatory oligonucletide libraries by an in vitro evolution processes, which possess high recognition ability [8]. Furthermore, they show high binding affinity, facile preparation, excellent stability, simple labeling and design flexibility [9], which make them very suitable for PDGF-BB detection. Electrochemical assays based on aptamers have been widely used for protein detection due to good selectivity and high sensitivity [10].

Recently, signal amplification strategies have been widely used in electrochemical biosensor in order to reduce the detection limit [11], mainly including nanoparticle tags [4], metal ions [12], electron transfer mediator [13] and biological amplification techniques [14,15]. Among them, biological amplification techniques based on nucleic acids, such as polymerase chain reaction [16], strand displacement amplification (SDA) [17], exonuclease III assisted target recycling [18] and

hybridization chain reaction [19], have been paid great attention due to high selectivity and sensitivity. Recently, the secondary structures of nucleic acids including hairpin [20], G-quadruplex [13], hand-in-hand [21] and cruciform [22] have also been used in electrochemical biosensors. Thereinto, Y-DNA contains three single-strand DNAs which are partially complementary to each other. Owing to its structural flexibility and conformational stability, Y-DNA can be projected to have various functional groups to fabricate various aptasensors [23,24]. Furthermore, Y-DNA has an important effect upon supramolecular nanostructures with manageable size, topology, and stability of its building units [25,26].

Hemin/G-quadruplex [27] has been employed to construct sensitive electrochemical biosensors. It can act as horseradish peroxidase-mimicking DNAzyme and therefore overcomes disadvantages of protein enzyme. Furthermore, it can serve as catalyst and electron transfer medium. In the hemin/G-quadruplex, hemin directly works as an electroactive molecule [28], which is helpful to improve the electrochemical performance of the biosensor due to the oxidation of Fe(II) in hemin.

On the other hand, nanomaterials have been widely used in electrochemical biosensor, such as metal nanoparticles, carbon, metal sulfide and polymers. They not only can improve the electrochemical response, but also can enhance immobilization of biomolecules on the biosensor [29]. In the last decade, graphene and carbon nanotubes have been broadly applied for fabricating high-performance electrochemical biosensors due to their high surface area, superior electronic conductivity and excellent mechanical strength [30,31]. Se element has much higher

intrinsic electrical conductivity than S [32]. Au nanoparticles (AuNPs) are mostly used in the fabrication of electrochemical biosensor because they have good conductivity and can immobilize biomolecule by Au-S bond.

In this work, a sensitive electrochemical biosensor is developed for PDGF-BB detection based on Se doped multi-walled carbon nanotubes (MWCNTs)-graphene hybrids (Se-MWCNTs-graphene), AuNPs, Y-shaped DNA-aided target recycling signal amplification and hemin/G-quadruplex. Aptamer was designed to contain thiol in its sequence. The aptamer was first immobilized on the electrode by Au-S interaction. When PDGF-BB was added, aptamer binded with it and triggered catalytic assembly of two other hairpins DNAs to form G-quadruplex Y-junction DNA structures, which released target PDGF-BB to again bind the intact aptamer to initiate another assembly cycle. After that, G-quadruplex/hemin complexes were produced when hemin was added to generated substantially amplified current output.

2. Experimental

2.1. Chemicals

Graphite powder, 6-mercapto-hexanol (MCH), $KMnO_4$ and diphenyl diselenide were obtained from Sigma Aldrich (St. Louis, MO). Thrombin (TB), immunoglobin G (IgG), prostate-specific antigen (PSA) were purchased from Sigma-Aldrich (Shanghai, China). Hemin bovine and PDGF-BB were obtained from Shanghai Xueman Biotechnology Co. Ltd (Shanghai, China). DNA sequences were designed

according to the reference [14] and prepared by Shanghai Sangon Biological Engineering Technology Co. Ltd (Shanghai, China). Their sequences are as follows:

H1: 5-SH-$(CH_2)_6$-CAGGCTACGGCACGTAGAGCATCACCATGATCCTGTAGC CTGCCTACATCAGGATCATGGTGAATGGGTA-3

H2: 5-TGGGTAGGGCGGGTCACCATGATCCTGATGTAGGCAGGCTATGCTC TACGTGCCGTAGCCTGCCTACATAGGGT-3

H3: 5-TGGGTAGGGCGGGTATGTAGGCAGGCTACGGCACGTAGAGCACAG GATCATGGTGATGCTCTACGTGCCGTAGCCTG-3

2.2. Apparatus

The morphologies of products were observed by a scanning electron microscopy (SEM, JSM-6510) (JEOL Ltd., Japan) and a transmission electron microscopy (TEM, JEM-2100F). The energy dispersive spectrum (EDS) analysis was attached to SEM for exploring elementary component. An X-ray powder diffraction (X'Pert-Pro MPD) and a Renishaw Raman system model 1000 spectrometer (Gloucestershire, UK) were also applied to characterize the samples.

2.3. Preparation of Se-doped MWCNTs-graphene hybrids

Graphene oxide was synthesized by modified Hummer's method [33]. MWCNTs were pretreated according to reference [34] in a concentrated sulfuric acid-nitric acid mixture (3 : 1 v/v). 5 mg MWCNTs and 5 mg GO were then dispersed in 50 mL ethanol. Subsequently, 5 mg diphenyl diselenide was added with 50 min ultrasonic

process at 100 W. The mixture was then dried at 40 °C. After that, the obtained solid was annealed at 900 °C under argon atmosphere. After cooled to room temperature, the black Se-MWCNTs-graphene was isolated and characterized with EDS and XPS.

2.4. Fabrication of biosensor and electrochemical detection

Glassy carbon electrode (GCE) was first treated by alumina slurry. After that, 8 μL Se-MWCNTs-graphene suspension (1 mg mL^{-1}) was applied on it. After washed with water and dried in the air, the electrode was dipped in 0.1% $HAuCl_4$ solution containing 0.1 M KNO_3 to perform electro-deposition of AuNPs at a constant potential of -0.2 V for 60 s. Then, 8 μL buffer (10 mM Tris-HCl,1 mM EDTA, 10 mM TCEP, 1 mM $MgCl_2$, 0.1 M NaCl, pH 7.4) containing 1 μM H1 was applied on the electrode and incubated for 12 h. 8 μL MCH (1 mM) was then applied on electrode and incubated for 120 min. Afterward, the electrode was incubated in the solution containing PDFG-BB, H2 (1 μM) and H3 for 30 min at 37 °C. Finally, the resultant electrode was incubated in 10 μL of hemin (5 μM) for 30 min.

Electrochemical test was carried out on a RST5200F electrochemical workstation (Zhengzhou Shi Rui Si Instrument, China). A three-electrode system was used with platinum wire as auxiliary electrode and Ag/AgCl as reference electrode. CV and EIS were detected in a mixture of 1 mM potassium ferricyanide and 0.1 M potassium chloride. DPV was carried out in 0.1 M PBS (pH 7.4) with pulse amplitude of 0.005 V, pulse width of 0.05 s and the pulse period of 0.2 s.

3. Results and discussion

3.1. Design strategy

Scheme 1 shows working principle of Y-shaped DNA-aided target recycling signal amplification strategy. Se-MWCNTs-graphene is first immobilized on the electrode and then AuNPs are electrodeposited upon it to act as supporting substrate. Aptamer is designed to contain thiol in its sequence. The aptamer-containing hairpin probes H1 are first immobilized on the electrode by Au-S interaction. When PDGF-BB is added, H1 binds with PDGF-BB to produce aptamer/PDGF-BB complex and open its hairpin structure. Subsequently, it partly hybridizes with H2 and releases the assembly initiation sequence in H2 by forming partial double-strand DNA. The remained sequence of the unfolded H2 further hybridizes with H3 to initiate another strand displacement reaction to displace the target PDGF-BB and forms the DNA Y-junction structures. The released target PDGF-BB can again bind the intact H1 to initiate another assembly cycle, which results in the generation of vast G-quadruplex Y-junction DNA structures. When hemin and K^+ are added, the G-quadruplex Y-junction brings the split G-quadruplex into proximity to produce G-quadruplex/hemin complexes..

3.2. Characterization

The SEM images in Fig. 1A exhibits the morphologies of the Se-MWCNTs-graphene hybrids. The graphene displays well thin-sheet structure with MWCNTs twining among the sheets. Fig. 1B shows the TEM image of Se-MWCNTs-graphene

hybrids. It can be clearly observed that the MWCNTs intersperse graphene in the hybrids.

The elementary composition of Se-MWCNTs-graphene hybrids was also studied by EDS analysis (Fig. 1C). The spectrogram shows the presence of C, O and Se elements. The amount of Se in the hybrids is 11.92% (wt.%). XPS characterization was also applied for elemental analysis of Se-MWCNTs-graphene hybrids. As presented in Fig. 1D, the characteristic peaks of Se3d, O1s and C1s are clearly observed in the full region of Se-MWCNTs-graphene hybrids. The EDS and XPS results ascertain the successful preparation of Se-MWCNTs-graphene hybrids.

The Raman spectrum of Se-MWCNTs-graphene and MWCNTs are presented in Fig. 2E. The *D* peak at 1352 cm^{-1} (corresponds to the presence of disorder in the hexagonal graphite layers) and *G* peak at 1591 cm^{-1} (in-plane bond stretch of C sp^2) can be observed clearly. The I_D/I_G intensity ratio of the Se-MWCNTs-graphene (2.52) is higher than the corresponding value of the MWCNTs-graphene (1.22), owing to difference in bond length and angles. X-ray diffraction patterns of Se-MWCNTs-graphene and MWCNTs are shown in Fig. 2F. The Se-MWCNTs-graphene exhibits a broad diffraction peak centering at 26.3°, which corresponds to graphitic (002) face. Furthermore, peak of 44.5° is ascribed to (110) peak of Fe residuals.

3.3. Electrochemical characterization

Different electrodes were studied by CV and EIS. Two well-defined redox peaks are obtained on GCE (Fig. 2A, curve a). The peak currents greatly increase

when Se-MWCNTs-graphene is applied on the GCE (curve b) due to it can create more active sites and significantly enhance the electron transfer rate. After AuNPs are electrodeposited on Se-MWCNTs-graphene/GCE (curve c), electrochemical signal further increases, because AuNPs can accelerate the electron transfer. Significant decrease in peak current appears after H1 (curve d) and MCH (curve e) are applied on the electrode respectively, because they obstructs the channel of electron transport and electron transfer becomes difficult. After H2, H3 and PDGF-BB are further applied on the electrode, current responses greatly decrease (curve f). The reason is double-strand DNA has more negative charged. After the addition of hemin, peak current further decreases (curve g) as the non-conductive hemin covering the surface of electrode. These results indicates that the biosensor is fabricated as expected.

Fig. 2B exhibits EIS results of various modification process of biosensor. Clearly, the R_{ct} of bare GCE is very small (curve a). After Se-MWCNTs-graphene and AuNPs are applied on the GCE, the R_{ct} decreases greatly (curve b and c), which shows almost line in EIS, suggesting good conductivity. When the thiol-modified H1 and MCH are further applied on electrode, R_{ct} increases obviously (curve d and e). Notably, the introduce of H2, H3, and PDGF-BB to the electrode causes a big R_{ct} (curve f) due to the generation of many double-strand DNA. Finally, when hemin is added, R_{ct} further enhances (curve g) because hydrophobic hemin blocks the active sites.

For demonstrating the signal amplification of Se-MWCNTs-graphene, CVs of

different electrodes in 1 mM potassium ferricyanide are recorded (Fig. 2C). The Se-MWCNTs-graphene modified GCE (curve e) displays the biggest redox peak currents among GCE，MWCNTs/GCE, graphene/GCE and MWCNTs-graphene/GCE (curves a-d), indicating its good electrochemical properties.

3.4. Optimization

The effect of incubation time of H2, H3 and PDFG-BB was evaluated (Fig. S1A). The DPV signal enhances rapidly when incubation time increases from 10 to 120 min. The current responses keep almost unchanged in the range of 120-180 min. Thus, 120 min was used in the further experiments.

The influence of H1 concentration on the DPV signal was studied. As shown in Fig. S1B, the current signal gradually enhances with the increase of the concentration of H1 from 0.1 to 1 μM and then decreases when the concentration is higher than 1 μM. Therefore, the concentration of H1 of 1 μM was used.

3.5. Signal amplification of the Y-shaped DNA + hemin/G-quadruplex system

The signal-amplification effect of the Y-shaped DNA + hemin/G-quadruplex system was studied. As shown in Fig. 3, the pure buffer only shows a negligible DPV response (curve a). Similarly, the H2 + H3 system can not result in the enhancement of current signal (curve b). The reason is that there is no G-quadruplex/hemin complex in the system in the absence of PDFG-BB. Nevertheless, the biosensor shows a small increase in the peak current (curve c) in the presence of PDFG-BB. It mainly comes from the reaction of PDFG-BB and aptamer, which can fold the aptamer in G-quadruplex and then interacts with hemin to produce current signal.

When the biosensor reacts with PDFG-BB + H2, the current response further increases because the unfolded H1 hybridizes with H2 to produce G-quadruplex/hemin complexes (curve d). More importantly, the coexistence of PDFG-BB, H2 and H3 shows a great enhancement in current response (curve e) because the formation of the G-quadruplex Y-junction structures can bind abundant hemin molecules.

3.6. Analytical performance of biosensor

The performance of the aptasensor were studied under the optimal conditions. The current signal increases with the increase of PDGF-BB concentration (Fig. 4A). The dependence of current signal on PDGF-BB concentration is exhibited in Fig. 4B. A linear range of 0.0001-10 nM toward PDGF-BB was obtained with a detection limit of 27 fM (S/N=3). The linear regression equation was i = -4.68 log (c/M)-65.14 (R = 0.997). The analytical performance of other PDGF-BB biosensors is listed in Table S1. The proposed aptasensor shows superior properties.

3.7. Specificity, reproducibility and stability

1 nM of TB, IgG and PSA were detected by the developed biosensor to evaluate its specificity. As shown in Fig. 4C, the presence of PDGF-BB induces a big current signal, whereas the addition of interferents has negligible effect on the current signal. Similarly, a mixed sample (1 nM PDGF-BB coexisting with 1 nM interfering components (TB, IgG and PSA)) does not result in obvious change in peak current compared to pure PDGF-BB, indicating good specificity of the proposed biosensor.

The reproducibility of the proposed biosensor was evaluated. Six proposed biosensors were prepared and used to detect 1.5 pM PDGF-BB. 4.5% of RSD was obtained, indicating good reproducibility. Moreover, the stability of developed biosensor was studied by keeping it under 4 ˚C for 4 weeks and then tested the electrochemical signal of 1.5 pM PDGF-BB. 92.8% initial current signal was obtained, indicating good stability. The good performance was due to large specific surface area of Se-doped MWCNTs-graphene hybrids and the stable hemin/G-quadruplex structure.

3.8. Serum samples analysis

To evaluate its application, the proposed aptasensor was used to detect PDGF-BB in the human serum. Six serum samples, three from healthy individuals and three from patients with hepatic fibrosis, were obtained from the affiliated hospital of Xinyang Normal University. The samples were detected by the proposed electrochemical aptasensor with one human EIA Kit as reference. Relative low errors (3.9-6.0%) between the developed biosensor and ELISA method indicates good accuracy of the aptasensor (Table S2). Therefore, this proposed biosensor can be applied to detect PDGF-BB in real samples.

4. Conclusions

In conclusion, a sensitive electrochemical aptasensor for selective determination of PDGF-BB is developed by using Se-doped MWCNTs-graphene hybrids, hemin/G-quadruplex and Y-shaped DNA probe target-triggered amplification strategy. The Se-doped MWCNTs-graphene hybrids harbor a high capacity of loading DNA probe and

can be used for signal development in aptasensor. In addition, the presence of PDGF-BB can trigger catalytic assembly formation of many G-quadruplex-containing Y-junction structures on the surface of the sensor electrode. The G-quadruplex captures hemin to produce greatly improved current signal to obtain completely label-free and sensitive detection of PDGF-BB down to 27 fM. Strikingly, the proposed assay can be easily operated and the matrix separated from the complex real sample containing another proteins that act as interference. All these results display an excellent specificity and high sensitivity in actual samples. Moreover, the biosensor can be employed to detect different targetss by changing the appropriate aptamers.

Acknowledgments

This work was supported by the National Natural Science Foundation of China (21475115), Program for University Innovative Research Team of Henan (15IRTSTHN001), Henan Provincial Science and technology innovation team (C20150026), Nanhu Scholars Program of XYNU, Nanhu Scholars Program for Young Scholars of XYNU, Natural Science Foundation of Henan Province (162300410230) and Henan Science and Technology Cooperation Project (172106000064).

References

[1] K.J. Huang, H.L. Shuai, J.Z. Zhang, Ultrasensitive sensing platform for platelet-derived growth factor BB detection based on layered molybdenum selenide–graphene composites and Exonuclease III assisted signal amplification, Biosens. Bioelectron. 77 (2016) 69-75, https://doi.org/10.1016/j.bios.2015.09.026.

[2] C. Betsholtz, B. Westermark, B. Ek, C.H. Heldin, Coexpression of a PDGF-like growth factor and PDGF receptors in a human osteosarcoma cell line: implications for autocrine receptor activation, Cell 39 (1984) 447-457, https://doi.org/10.1016/0092-8674(84)90452-5.

[3] S.X. Gao, X. Zheng, J.H. Wu, A biolayer interferometry-based enzyme-linked aptamer sorbent assay for real-time and highly sensitive detection of PDGF-BB, Biosens. Bioelectron. 102 (2018) 57-62, https://doi.org/10.1016/j.bios.2017.11.017.

[4] H. Li, Y.J. Zhao, Z. Chen, D.K. Xu, Silver enhanced ratiometric nanosensor based on two adjustable fluorescence resonance energy transfer modes for quantitative protein sensing, Biosens. Bioelectron. 87 (2017) 428-432, https://doi.org/10.1016/j.bios.2016.08.075.

[5] L.Y. Yao, X.Q. Yu, Y.J. Zhao, A.P. Fan, An aptamer-based chemiluminescence method for ultrasensitive detection of platelet-derived growth factor by cascade amplification combining rolling circle amplification with hydroxylamine-enlarged

gold nanoparticles, Anal. Methods 7 (2015) 8786-8792, https://doi.org/10.1039/c5ay01953b.

[6] C.C. Chang, S.C. Wei, T.H. Wu, C.H. Lee, C.W. Lin, Aptamer-based colorimetric detection of platelet-derived growth factor using unmodified goldnanoparticles, Biosens. Bioelectron. 42 (2013) 119-123, https://doi.org/10.1016/j.bios.2012.10.072.

[7] X. Liu, H.L. Shuai, K.J. Huang, A label-free electrochemical aptasensor based on leaf-like vanadium disulfide-Au nanoparticles for the sensitive and selective detection of platelet-derived growth factor BB, Anal. Methods 7 (2015) 8277-8284, https://doi.org/10.1039/C5AY01793A.

[8] L. Hong, F. Zhou, D. Shi, X. Zhang, G. Wang, Portable Aptamer Biosensor of Platelet-Derived Growth Factor-BB Using a Personal Glucose Meter with Triply Amplified, Biosens. Bioelectron. 95 (2017) 152-159, https://doi.org/10.1016/j.bios.2017.04.023.

[9] S. Bi, B. Luo, J. Ye, Z. Wang, Label-free chemiluminescent aptasensor for platelet-derived growth factor detection based on exonuclease-assisted cascade autocatalytic recycling amplification, Biosens. Bioelectron. 62 (2014) 208-213, https://doi.org/10.1016/j.bios.2014.06.057.

[10] A.A. Ensafi, E. Khoddami, B. Rezaei, Aptamer@ Au-o-phenylenediamine modified pencil graphite electrode: A new selective electrochemical impedance biosensor for the determination of insulin, Colloid. Surface. B. 159 (2017) 47-53, https://doi.org/10.1016/j.colsurfb.2017.07.076.

[11] Y.X. Chen, K.J. Huang, L.L. He, Y.H. Wang, Tetrahedral DNA probe coupling with hybridization chain reaction for competitive thrombin aptasensor, Biosens. Bioelectron. 100 (2018) 274-281, https://doi.org/10.1016/j.bios.2017.09.022.

[12] C. Ma, H. Liu, L. Zhang, H. Li, M. Yan, X. Song, J. Yu, Multiplexed aptasensor for simultaneous detection of carcinoembryonic antigen and mucin-1 based on metal ion electrochemical labels and Ru $(NH_3)_6^{3+}$ electronic wires, Biosens. Bioelectron. 99 (2018) 8-13, https://doi.org/10.1016/j.bios.2017.07.031.

[13] J. Wang, J. Guo, J. Zhang, W. Zhang, Y. Zhang, RNA aptamer-based electrochemical aptasensor for C-reactive protein detection using functionalized silica microspheres as immunoprobes, Biosens. Bioelectron. 95 (2017) 100-105, https://doi.org/10.1016/j.bios.2017.04.014.

[14] G. Wang, S. Wang, C. Yan, G. Bai, Y. Liu, DNA-functionalized gold nanoparticle-based fluorescence polarization for the sensitive detection of silver ions. Colloid. Surface. B. 167 (2018) 150-155, https://doi.org/10.1016/j.colsurfb.2018.04.004.

[15] H.L. Shuai, X. Wu, K.J. Huang, Molybdenum Disulfide Spheres-based Electrochemical Aptasensor for Proteins Detection, J. Mater. Chem. B 5 (2017) 5362-5372, https://doi.org/10.1039/C7TB01276D.

[16] A.B. Aysan, Z. Knejzlík, P. Ulbrich, M. Šoltys, A. Zadražil, F. Štěpánek, Effect of surface functionalisation on the interaction of iron oxide nanoparticles with

polymerase chain reaction, Colloid. Surface. B. 153 (2017) 69-76, https://doi.org/10.1016/j.colsurfb.2017.02.005.

[17] Y.X. Chen, K.J. Huang, F. Lin, L.X. Fang, Ultrasensitive electrochemical sensing platform based on graphene wrapping SnO_2 nanocorals and autonomous cascade DNA duplication strategy, Talanta 175 (2017) 168-176, https://doi.org/10.1016/j.talanta.2017.07.042.

[18] K.J. Huang, Y.J. Liu, Q.F. Zhai, Ultrasensitive biosensing platform based on layered vanadium disulfide-graphene composites coupling with tetrahedron-structured DNA probes and exonuclease III assisted signal amplification, J. Mater. Chem. B 3 (2015) 8180-8187, https://doi.org/10.1039/C5TB01239B.

[19] H.L. Shuai, X. Wu, K.J. Huang, Z.B. Zhai, Ultrasensitive electrochemical biosensing platform based on spherical silicon dioxide/molybdenum selenide nanohybrids and triggered Hybridization Chain Reaction, Biosens. Bioelectron. 94 (2017) 616-625, https://doi.org/10.1016/j.bios.2017.03.058.

[20] A. Kamal, Z. She, R. Sharma, H.B. Kraatzm, A study of the interactions of Hg (II) with TT mispair containing hairpin loops, Electrochim. Acta 243 (2017) 44-52, https://doi.org/10.1016/j.electacta.2017.05.058.

[21] C. Li, Z.Y. Wang, T. Gao, A.P. Duan, G.X. Li, Fabrication of hand-in-hand nanostructure for one-step protein detection, Chem. Commun. 49 (2013) 3760-3762, https://doi.org/10.1039/C3CC40543E.

[22] H. Kurahashi, H. Inagaki, K. Yamada, T. Ohye, M. Taniguchi, B.S. Emanuel, T. Toda, Cruciform DNA structure underlies the etiology for palindrome-mediated human chromosomal translocations, J. Biol. Chem. 279 (2004) 35377-35383. https://doi.org/10.1074/jbc.M400354200.

[23] M. Chen, N. Gan, T. Li, Y. Wang, Q. Xu, Y. Chen, An electrochemical aptasensor for multiplex antibiotics detection using Y-shaped DNA-based metal ions encoded probes with NMOF substrate and CSRP target-triggered amplification strategy, Anal. Chim. Acta 968 (2017) 30-39, https://doi.org/10.1016/j.aca.2017.03.024.

[24] J. Jia, H.G. Chen, J. Feng, J.L. Lei, H.Q. Luo, N.B. Li, A regenerative ratiometric electrochemical biosensor for selective detecting Hg^{2+} based on Y-shaped/hairpin DNA transformation, Anal. Chim. Acta 908 (2016) 95-101, https://doi.org/10.1016/j.aca.2015.12.028.

[25] Y.H. Roh, R.C.H. Ruiz, S.M. Peng, J.B. Lee, D. Luo, Engineering DNA-based functional materials, Chem. Soc. Rev. 40 (2011) 5730-5744, https://doi.org/10.1039/C1CS15162B.

[26] S. Chatterjee, J.B. Lee, N.V. Valappil, D. Luo, V.M. Menon, Probing Y-shaped DNA structure with time-resolved FRET, Nanoscale 4 (2012) 1568-1571, https://doi.org/10.1039/C2NR12039A.

[27] A. De Rache, I. Kejnovská, C. Buess-Herman, T. Doneux, Electrochemical and circular dichroism spectroscopic evidence of two types of interaction between [Ru

$(NH_3)_6]^{3+}$ and an elongated thrombin binding aptamer G-quadruplex, Electrochim. acta 179 (2015) 84-92, https://doi.org/10.1016/j.electacta.2015.05.023.

[28] Y.H. Wang, K.J. Huang, X. Wu, Y.Y. Ma, D.L. Song, C.Y. Du, S.H. Chang, Ultrasensitive supersandwich-type biosensor for enzyme-free amplified microRNA detection based on N-doped graphene/Au nanoparticles and hemin/G-quadruplexes, J. Mater. Chem. B 6 (2018) 2134-2142, https://doi.org/10.1039/C8TB00061A.

[29] Y.X. Chen, K.J. Huang, K.X. Niu, Recent advances in signal amplification strategy based on oligonucleotide and nanomaterials for microRNA detection-a review, Biosens. Bioelectron. 99 (2018) 612–624, https://doi.org/10.1016/j.bios.2017.08.036.

[30] P.P. Waifalkar, A.D. Chougale, P. Kollu, P.S. Patil, P.B. Patil, Magnetic nanoparticle decorated graphene based electrochemical nanobiosensor for H_2O_2 sensing using HRP, Colloid. Surface. B. 167 (2018) 425-431, https://doi.org/10.1016/j.colsurfb.2018.04.042.

[31] X. Zhao, K. Tian, T. Zhou, X. Jia, J. Li, P. Liu, PEGylated multi-walled carbon nanotubes as versatile vector for tumor-specific intracellular triggered release with enhanced anti-cancer efficiency: Optimization of length and PEGylation degree, Colloid. Surface. B. 2018, https://doi.org/10.1016/j.colsurfb.2018.02.041.

[32] Y.H. Wang, K.J. Huang, X. Wu, Recent advances in transition-metal dichalcogenides based electrochemical biosensors: A review, Biosens. Bioelectron. 97 (2017) 305-316, https://doi.org/10.1016/j.bios.2017.06.011.

[33] W.S. Hummers, R.E. Offeman, Preparation of graphitic oxide, J. Am. Chem. Soc. 80 (1958) 1339-1339, https://doi.org/10.1021/ja01539a017.

[34] Z.P. Jin, H.G. Nie, Z. Yang, J. Zhang, Z. Liu, X.J. Xu, S.M. Huang, Metal-free selenium doped carbon nanotube/graphene networks as a synergistically improved cathode catalyst for oxygen reduction reaction, Nanoscale 4 (2012) 6455-6460, https://doi.org/10.1039/C2NR31858J.

[35] H. Xu, S. Liang, X. Zhu, X. Wu, Y. Dong, H. Wu, W. Zhang, Y. Chi, Enhanced electrogenerated chemiluminescence behavior of C_3N_4 QDs@ C_3N_4 nanosheet and its signal-on aptasensing for platelet derived growth factor, Biosens. Bioelectron. 92 (2017) 695-701, https://doi.org/10.1016/j.bios.2016.10.026.

[36] J. Han, Y. Zhuo, Y.Q. Chai, R. Yuan, Y. Xiang, Q. Zhu, N. Liao, Multi-labeled functionalized C_{60} nanohybrid as tracing tag for ultrasensitive electrochemical aptasensing, Biosens. Bioelectron. 46 (2013) 74-79, https://doi.org/10.1016/j.bios.2013.02.020.

[37] L.J. Bai, R. Yuan, Y.Q. Chai, Y. Zhuo, Y.L. Yuan, Y. Wang, Simultaneous electrochemical detection of multiple analytes based on dual signal amplification of single-walled carbon nanotubes and multi-labeled graphene sheets, Biomaterials 33 (2012) 1090-1096, https://doi.org/10.1016/j.biomaterials.2011.10.012.

[38] M. Zou, D. Li, R. Yuan, Y. Xiang, A target-responsive autonomous aptamer machine biosensor for enzyme-free and sensitive detection of protein biomarkers, J. Mater. Chem. B 2018, https://doi.org/10.1039/C8TB00610E.

[39] K. Deng, Y. Xiang, L. Zhang, Q. Chen, W. Fu, An aptamer-based biosensing platform for highly sensitive detection of platelet-derived growth factor via enzyme-mediated direct electrochemistry, Anal. Chim. Acta 759 (2013) 61-65, https://doi.org/10.1016/j.aca.2012.11.018.

Figures

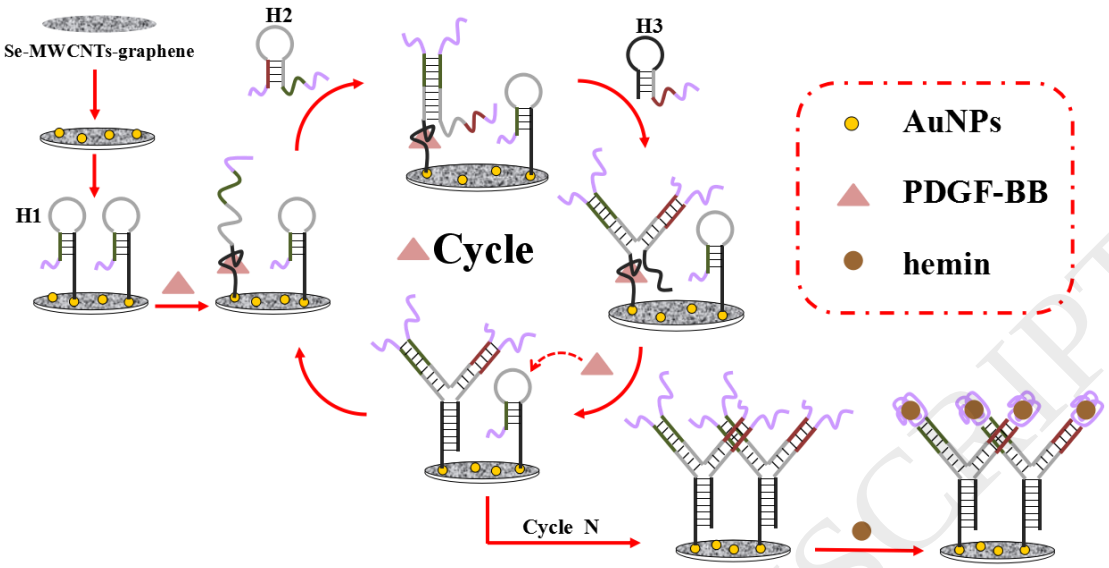

Scheme 1 Preparation of aptasensor.

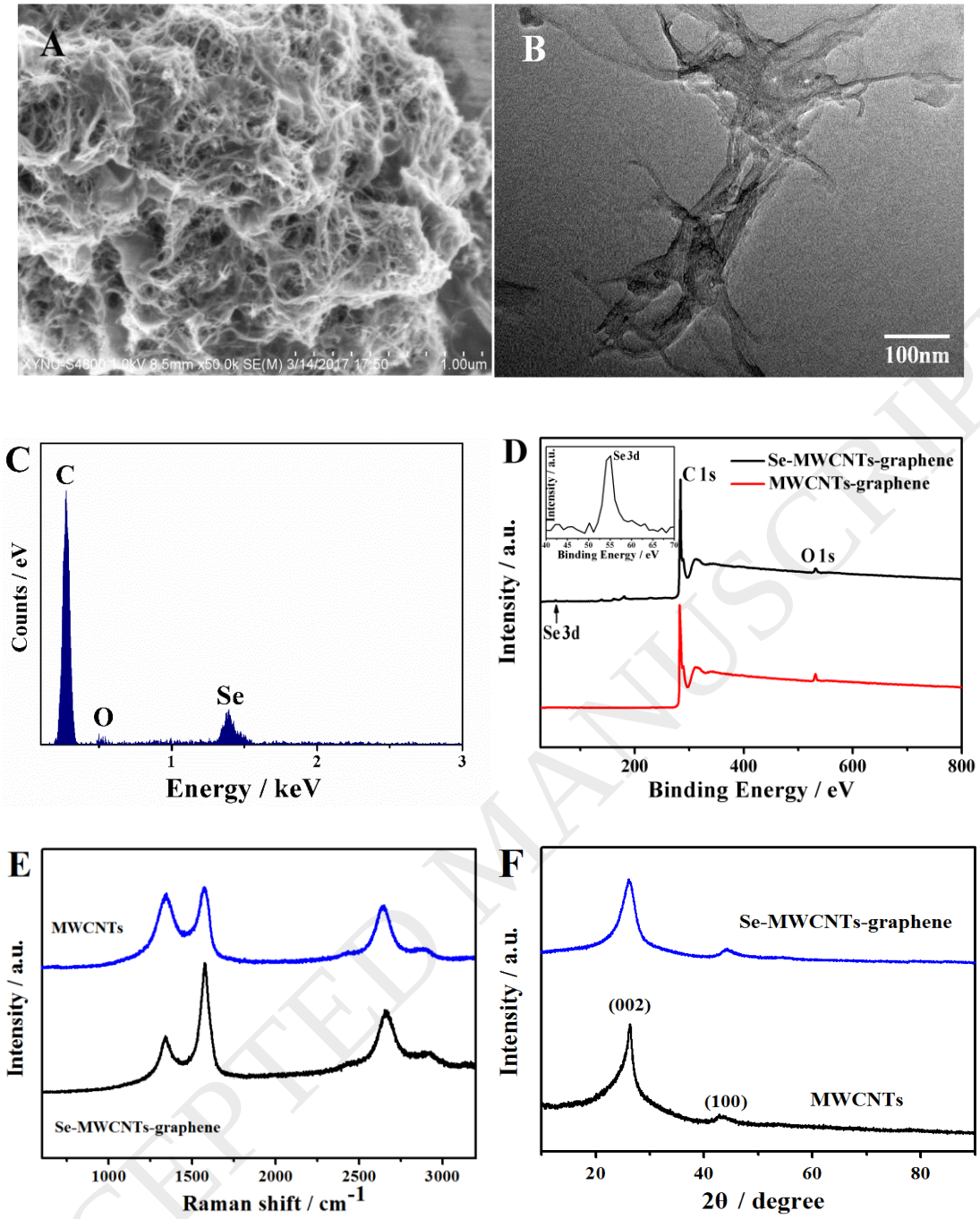

Fig. 1. SEM image (A), TEM image (B), EDXS (C) and XPS survey spectra of Se-MWCNTs-graphene (D); Raman spectrum (E) and XRD patterns (F) of MWCNTs-graphene and Se-MWCNTs-graphene.

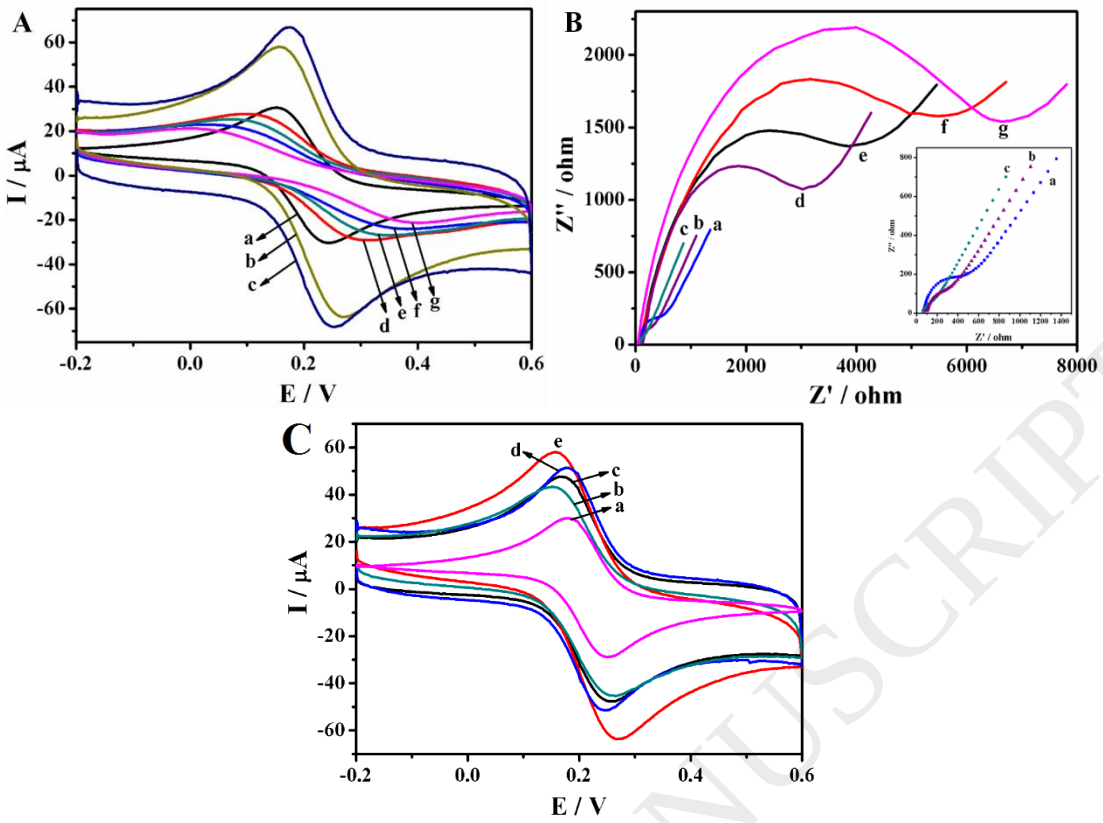

Fig. 2. (A) CV and (B) EIS of bare GCE (a), Se-MWCNTs-graphene/GCE (b), Au/Se-MWCNTs-graphene/GCE (c), H1/Au/Se-MWCNTs-graphene/GCE (d), MCH/Au/Se-MWCNTs-graphene/GCE (e), H2, H3, and PDGF-BB/MCH/Au/Se-MWCNTs-graphene/GCE (f), hemin/H2, H3, and PDGF-BB/MCH/Au/Se-MWCNTs-graphene/GCE (g); (C) CV of GCE (a), MWCNTs/GCE (b), graphene/GCE (c), MWCNTs-graphene/GCE (d), Se-MWCNTs-graphene/GCE (e).

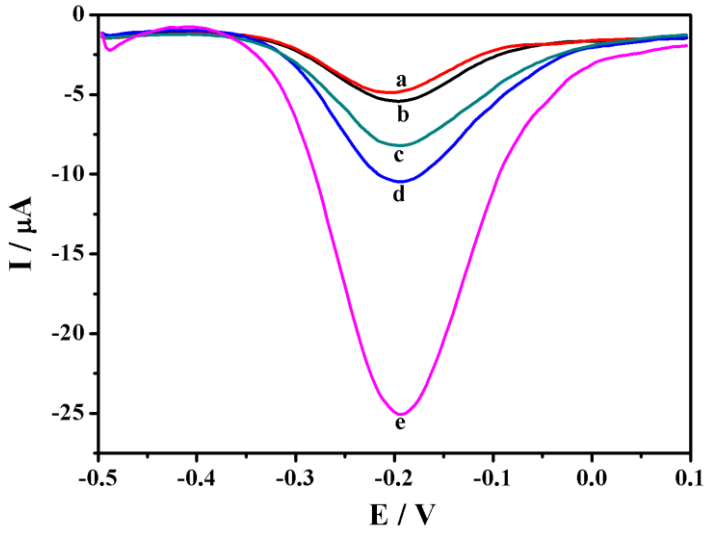

Fig. 3. DPV of buffer (a), H2 + H3 (b), PDGF-BB (c), PDGF-BB + H2 (d), PDGF-BB + H2 + H3 (e). The concentration of PDGF-BB is 1 nM, and those of H1, H2 and H3 are 1 μM.

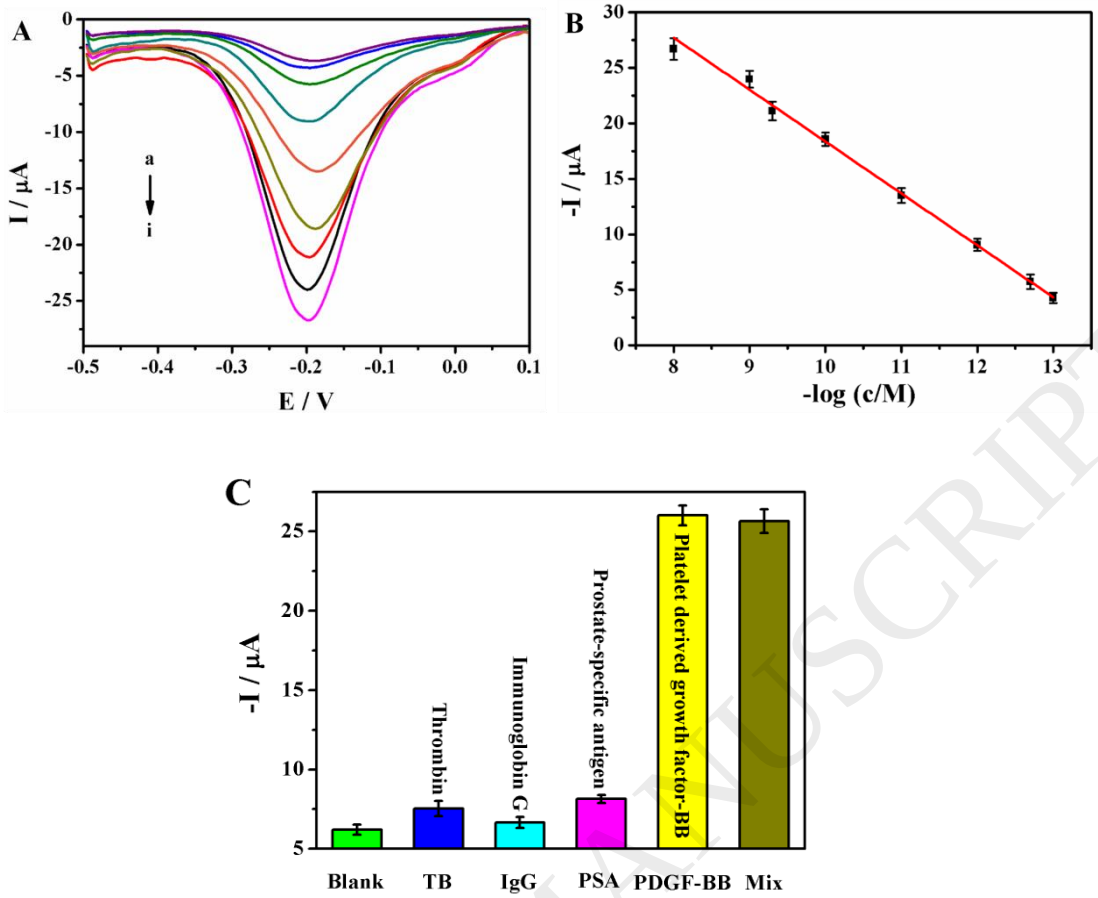

Fig. 4. (A) DPV of various PDFG-BB concentrations (from a to i): 0; 1×10^{-13}; 2×10^{-13}; 1×10^{-12}; 1×10^{-11}; 1×10^{-10}; 5×10^{-10}; 1×10^{-9}; 1×10^{-8} M, respectively; (B) calibration plot of the DPV current versus the logarithm concentration of PDFG-BB. Error bar shows the standard deviation (SD) of measurement taken from three independent experiments; (C) Anti-interference investigation of the proposed aptasensor for the target PDGF-BB (1 nM) against other control proteins of TB (1 nM), IgG (1 nM), PSA (1 nM) and the mixture (1 nM PDGF-BB, 1 nM TB, 1 nM IgG, 1 nM PSA).